Inorganic Chemistry

Article

pubs.acs.org/IC

Paramagnetic Hexacyanometalates. The Diversity of Spin Distribution Studied by ^{13}C and ^{15}N MAS NMR Spectroscopy

Natalia Baumgärtel,[†] Alexandrine Flambard,[‡] Frank H. Köhler,*[,†] and Rodrigue Lescouëzec[‡]

[†]Department Chemie, Technische Universität München, Garching 85748, Germany

[‡]Institut Parisien de Chimie Moléculaire, UMR 7201 Université Paris 6, 75252 Paris Cedex 05, France

Supporting Information

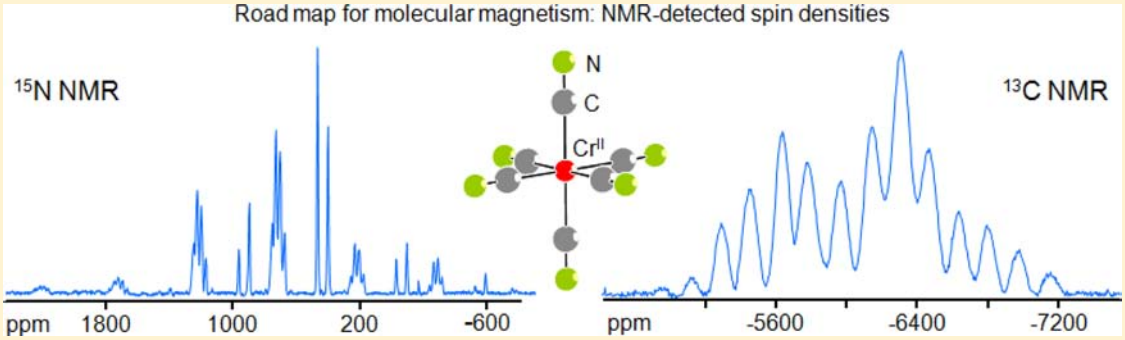

ABSTRACT: With the aim of probing the spin density distribution in the open-shell cyanometallates $Cs_2K[M(CN)_6]$ (M = Cr, Mn, Fe), $K_3[M(CN)_6]$ (M = Mn, Fe), $K_4[M(CN)_6]$ (M = Cr, Mn), and $K_4[V(CN)_7]$ have been studied by solid-state ^{13}C and ^{15}N NMR spectroscopy. The signals appear in strongly shifted and broad ranges (^{13}C, −2100 to −8900 ppm; ^{15}N, −1900 to 2400 ppm) except $K_4[V(CN)_7]$, which is NMR-silent. Analysis of the isotropic signal shifts yields negative spin density in all carbon 2s orbitals (up to 12.2% at the six ligands of $[Mn(CN)_6]^{3-}$) and positive spin density in all nitrogen 2s orbitals (up to 1.1% at the six ligands of $[Mn(CN)_6]^{4-}$ and $[Fe(CN)_6]^{3-}$). This is in accord with the induction of alternating spin at the CN ligands by successive polarization of σ bonds triggered by the spin center M^{n+}. The signal shift anisotropies are related to spin in the carbon and nitrogen $2p_\pi$ and $2p_\sigma$ orbitals. In the case of $Cs_2K[Cr(CN)_6]$ and $K_4[Cr(CN)_6]$ much positive spin is found in the nitrogen $2p_\pi$ orbitals, which corresponds to direct M → N spin transfer. On $Cs_2K[M(CN)_6]$ (M = Mn, Fe), the $2p_\pi$ spin density at nitrogen is negative. The results are in accord with and extend the data of polarized neutron diffraction and EPR spectroscopy. Owing to high signal resolution, small deviations of the $[M(CN)_6]^{n-}$ ions from octahedral symmetry and disorder of crystal layers have been detected. This corresponds to the crystal symmetry and to Jahn−Teller distortion. The disorder entails a scatter of spin densities. In the case of $K_4[Mn(CN)_6]$ it reaches 19% for the C 2s orbitals and 80% for the N 2s orbitals with regard to the respective smallest spin population.

INTRODUCTION

The chemistry of paramagnetic hexacyanometalates has experienced a renaissance, because these ions feature in many novel magnetically attractive materials. Prototypes are the bulk-magnetic Prussian blue analogues where spin alignment remains stable up to relatively high temperature and that can exist even above room temperature.[1] In recent studies, cyanometalate fragments have been used for building ionic clusters of paramagnetic transition metal centers, for designing nanomagnets in a bottom-up approach to superparamagnets and ferromagnets by selectively introducing CN bridges,[2] for assembling small clusters[3] as well as low-dimensional (in particular, 1D) magnets,[4] and for creating extended frameworks of bulk magnets.[5] Examples are molecular squares[6] and cubes[7] where CN ligands link various paramagnetic metal ions. These are approaches to new single-molecule magnets, which show magnetic ordering albeit at low temperatures or which are superparamagnets as in the case of ligand-protected Ni^{2+} ions linked to a Cr^{3+} center by CN bridges.[8] Recently, mixed-valent behavior has been established in molecular squares,[9] and CN-linkage isomerism has been found in a tetradecametallic cluster.[10] There are also photomagnetically active cyanometalates such as $CsFe[Co(CN)_6]$,[11] $[Mn(bipy)_2]_4[Mo(CN)_8]_2$,[12] $CsCu_7[Mo(CN)_8]_4(H_2O)_6$,[13] and $RbMn[Fe(CN)_6]$,[14] which are generally promising for the application in magneto-optical devices. High-spin clusters are another topic where cyanometalates play an important role.[15] Cyanide bridges in one-dimensional assemblies of transition-metal fragments furnish novel chain magnets,[16] and they are the key ligands in materials featuring spin crossover[17] or coexisting ferroelectric and ferromagnetic behavior.[18]

For designing and optimizing materials that are assembled from paramagnetic building blocks by systematically making

Received: July 16, 2013
Published: October 22, 2013

use of the arsenal of known magnetic interactions, key information is the distribution of unpaired electrons in the starting compounds. Of particular interest is the fraction of unpaired electrons, that is, the spin density, at ligand atoms, which are envisaged to figure as links to neighboring spin centers of a new magnetic material. This is also true for the cyanide-bridged materials mentioned above.[5,19] However, there are not many choices for experimentally studying spin density distributions in genuine materials that are magnetically undiluted solids. X-ray magnetic circular dichroism is a powerful method for determining the spin structure of the metal ions in molecule-based magnetic materials having a macroscopic magnetic moment.[20] But the spin distribution in building blocks, in particular the spin transfer to ligands, is not accessible. When single crystals are available polarized neutron diffraction (PND) is particularly well suited for spin density studies, and examples of cyanometalates studied so far are $[Fe(CN)_6]^{3-}$,[21] $[Cr(CN)_6]^{3-}$,[22] $[Mo(CN)_7]^{4-}$,[23] and $[Mo(CN)_8]^{3-}$ besides other fragments in $Mn_9Mo_6(CN)_{48}(CH_3OH)_{29}(H_2O)_2$.[15] But unfortunately, the PND data are often limited as will be discussed below. An alternative method is solid-state NMR spectroscopy because the signal shifts are a measure of the spin density at the nucleus under investigation.[24] Given the advantage that powder samples can be used in a relatively inexpensive experimental setup, we have started a research program for testing the method with the basic building blocks $[Cr(CN)_6]^{4-}$, $[Mn(CN)_6]^{4-}$, $[Cr(CN)_6]^{3-}$, $[Mn(CN)_6]^{3-}$, and $[Fe(CN)_6]^{3-}$. A preliminary report on the dicesium–potassium salts of the latter two anions has appeared.[25] In the present paper, we first resume the background of the method. Subsequently, the experimental results with emphasis on the NMR spectra are discussed followed by sections on the spin density distribution.

NMR signal shifts obtained from paramagnetic compounds provide access to spin densities, because they are related to the scalar (Fermi contact) coupling between the nucleus under study and the unpaired electrons.[24] Owing to fast electron relaxation, the coupling pattern to each nonequivalent nucleus is reduced to one signal whose shift is usually much larger than that known for diamagnetic compounds. The electron–nuclear coupling is also related to the spin density at the respective nucleus so that, in the end, the spin density at any nucleus of an open-shell compound can be expressed by the NMR signal shift as outlined in more detail below.

The access to spin densities via NMR spectroscopy is indirect, because (hyperfine) couplings are measured that are then linked to molecular orbitals. By contrast, the PND method more directly gains information on spatial spin distributions from diffraction patterns, but there are also limitations. The pros and cons of the magnetic resonance approaches have been discussed.[24,26] Since then, progress has been made in theoretically reproducing the NMR signal shifts of paramagnetic compounds.[27]

Relaxation may be a constraint of the NMR method. An important parameter acting on the line broadening is the distance, r, of the nucleus under study from the spin center (in this work, the transition metals, M). From the simple relation $\Delta\nu \propto 1/r^6$, where $\Delta\nu$ is the signal half width, one expects that for $[M(CN)_6]^{n-}$ ions, the signal resolution of ^{15}N NMR spectra would be better than that of ^{13}C NMR spectra, because the N atoms are about 1.15 Å more distant from M than are the C atoms. Checking the impact of these distances was hence another reason for studying both nuclei. Generally, the M–C bonds and the M···N distances seem unfavorably short. This disadvantage may be compensated by other parameters determining $\Delta\nu$, and a short electron relaxation time, τ_e, would be most helpful. Since τ_e cannot be well predicted in many cases, another aim of the study was to test the limit of NMR access of cyanometalates.

RESULTS AND DISCUSSION

Hexacyanomanganate(III) and -ferrate(III). The synthetic effort was mainly determined by the signal-to-noise ratio of the NMR spectra. Though solid-state ^{13}C NMR spectra at natural abundance could be obtained, the signal-to-noise ratio and the resolution were not satisfactory and prevented spectrum analysis. An example is given for $K_3[Mn(CN)_6]$ in the Supporting Information (Figure S1). Therefore, compounds selectively enriched in ^{13}C or ^{15}N were prepared. In order to keep the nuclear dipole interaction at a negligible level, $K^{13}CN$ and $KC^{15}N$ rather than $K^{13}C^{15}N$ were used as starting compounds. After optimization of the syntheses by use of isotopically nonenriched KCN, relatively good yields (40–95%) were obtained.

The powder samples of $K_3[Mn(CN)_6]$ and $K_3[Fe(CN)_6]$ used for solid-state NMR spectroscopy were made by grinding crystals. Typical magic angle spinning (MAS) spectra of

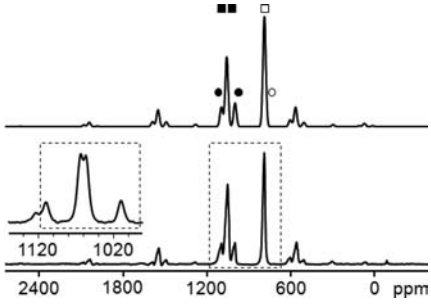

Figure 1. ^{15}N MAS NMR spectrum of $K_3[Mn(CN)_6]$: bottom, experimental, ν_r = 15 kHz, T = 331.8 K; inset ν_r = 5 kHz, T = 328.6 K; isotropic signals are framed; top, simulated (see data in Table S3, Supporting Information). For signal assignment, see text; polytype 1, □■■; polytype 2, ○●●; open and filled labels correspond to axial and equatorial CN ligands, respectively.

$K_3[Mn(CN)_6]$ are shown in Figures 1 and 2. The isotropic ^{15}N NMR signals appear between 1150 and 1470 ppm and are better resolved at a spinning frequency, ν_r, of 5 kHz (two

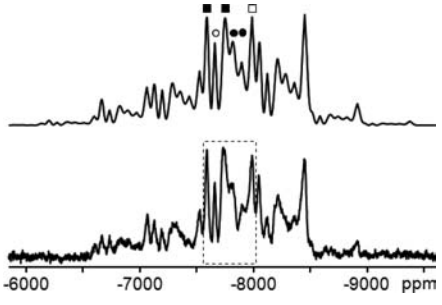

Figure 2. ^{13}C MAS NMR spectrum of $K_3[Mn(CN)_6]$: bottom, experimental, ν_r = 35 kHz, T = 326.4 K; isotropic signals are framed; top, simulated with the data given in Table S3, Supporting Information. For signal assignment, see text and Figure 1.

dx.doi.org/10.1021/ic401830f | Inorg. Chem. 2013, 52, 12634–12644

signals near 1420 ppm) than at 15 kHz (Figure 1). The spectra at these and other spinning frequencies could be well simulated, whereas attempts to reproduce the ^{13}C NMR spectra up to ν_r = 17 kHz were not satisfactory. Running the spectra above 30 kHz was a crucial improvement, and results as shown in Figure 2 were obtained. The simulation of spectra at different spinning frequencies yielded six isotropic signals with shifts between −7590 and −7990 ppm. For the signal assignment, the sideband spectra were integrated giving intensities that could be grouped in sets of three signals. For a given set, the intensities were similar although some scatter occurred, which was attributed to the limitations of signal deconvolution. The signal sets were assigned arbitrarily to different types of distorted hexacyanometalates. Each set had a pair of more or less adjacent signals, which were attributed to the equatorial CN ligands and the third signal was left for the axial CN ligand. This corresponds to what has been established for the Cs_2K salts.[25] This assignment procedure was also applied successfully to most of the other spectra below.

The MAS NMR spectra of $K_3[Fe(CN)_6]$ were similar to those of $K_3[Mn(CN)_6]$, but there were also differences. Again the resolution of the ^{15}N NMR spectrum (Figure 3) was better

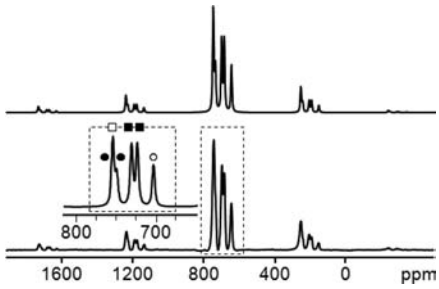

Figure 3. ^{15}N MAS NMR spectrum of $K_3[Fe(CN)_6]$: bottom, experimental, ν_r = 15 kHz, T = 326.3 K; inset ν_r = 7.5 kHz, T = 326.4 K; isotropic signals are framed; top, simulated with the data given in Table S4, Supporting Information. For signal assignment, see text and Figure 1.

at lower spinning frequencies, and five isotropic signals were obtained. The intensities were in accord with two sets of signals for distorted $[Fe(CN)_6]^{3-}$ ions; one of the low-intensity signals coincided with the high-intensity signal at 1107 ppm. By contrast, in the ^{13}C NMR spectrum (Figure 4) only one broad signal appeared, which showed some structure when the sample was spun faster than 30 kHz. Signal deconvolution (Figure S2, Supporting Information) pointed to more than four signals, but

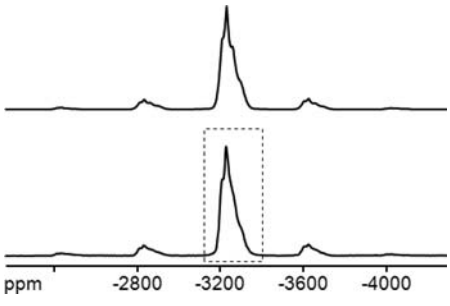

Figure 4. ^{13}C MAS NMR spectrum of $K_3[Fe(CN)_6]$: bottom, experimental, ν_r = 30 kHz, T = 326.3 K; isotropic signals are framed; top, simulated with the data given in Table S4, Supporting Information.

only those clearly visible as shoulders were considered for the data summary of $K_3[Mn(CN)_6]$ and $K_3[Fe(CN)_6]$ in Tables S3 and S4, Supporting Information. Further assignment to axial and equatorial CN ligands of different $[Fe(CN)_6]^{3-}$ ions was too speculative.

Surprisingly, $K_3[Mn(CN)_6]$ and $K_3[Fe(CN)_6]$ gave up to six isotropic signals although only up to three were expected for distorted octahedra as actually found for $Cs_2K[Mn(CN)_6]$ and $Cs_2K[Fe(CN)_6]$.[25] Also, the signal intensities did not correspond to the 1/1/1 pattern expected for two different equatorial and one axial CN group or to the 1/2 pattern of an axial and nonresolved equatorial CN groups. These features actually portray the crystal structure of the series $K_3[M(CN)_6]$ where M is Cr,[28] Mn,[29] Fe,[30] and Co[31] (for a more complete listing, see ref 9a). These compounds exhibit polytypism with the basic structure being monoclinic. The polytypes result from stacking layers[31a] of monoclinic unit cells as shown for the simplest case in Figure 5. When two unit cells of alternating

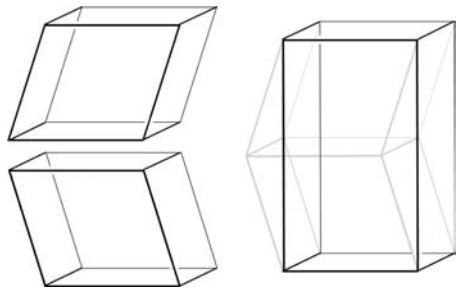

Figure 5. The origin of polytypism in the series $K_3[M(CN)_6]$: Stacking of, for instance, two monoclinic unit cells (left) yields an orthorhombic unit cell (right).

adjacent layers (Figure 5, left) are fused as shown in Figure 5 on the right, an orthorhombic two-layer unit cell is created. Further stacking of layers would ideally lead to monoclinic three-layer, orthorhombic four-layer, and monoclinic five-layer structures and so forth. However, although one- through four- and seven-layer structures have been established, real samples are often more complicated, because twinning[28b,29b] and layer disorder[28b,29a] may interfere. Also, if polycrystalline samples are prepared they would probably contain more than one polytype. For $K_3[Mn(CN)_6]$ and $K_3[Fe(CN)_6]$ investigated here, only monoclinic one-layer and orthorhombic two-layer polytypes have been observed at room temperature.[29,30] Hence we conclude that these two polytypes are seen in the MAS NMR spectra. When the signal resolution is sufficient, the polytypes may be distinguished as in the case of $K_3[Mn(CN)_6]$. There are two sets of sideband spectra whose intensity ratio is roughly 2/1 with some scatter owing to signal overlap (Table S3, Supporting Information). It follows that one polytype is more abundant than the other. While further assignment to one-layer and two-layer polytypes is unclear, their axial and equatorial CN ligands can be distinguished as mentioned above.

Hexacyanochromate(III) and Heptacyanovanadate-(III). After optimization of the syntheses by use of nonenriched KCN, microcrystalline $Cs_2K[Cr(^{13}CN)_6]$, $Cs_2K[Cr(C^{15}N)_6]$, and $K_4[V(C^{15}N)_7]$ were obtained in good to moderate yield (52% and 21%, respectively). Single crystals of the vanadium compound have been reported to contain two molecules of water, but compounds with less water and even free of water have also been obtained.[32] The sample used for the present study analyzed as $K_4[V(C^{15}N)_7](H_2O)_{1.2}$.

dx.doi.org/10.1021/ic401830f | Inorg. Chem. 2013, 52, 12634−12644

^{13}C MAS NMR experiments were performed in ranges up to about ±50 000 ppm relative to the diamagnetic signal shift range, but no signals could be found for $Cs_2K[Cr(CN)_6]$. The same applied for the ^{15}N MAS NMR spectrum of $K_4[V(CN)_7]$. Obviously, the $[Cr(CN)_6]^{3-}$ and $[V(CN)_7]^{4-}$ ions suffer from fast nuclear relaxation, which broadens the signals beyond the detection limit. This is surprising, because useful ^{1}H and ^{13}C NMR spectra have been obtained previously for other compounds featuring Cr(III) $S = 3/2$[33] and V(III) $S = 1$[34] ions. The discrepancy is thought to be due to different electron relaxation times, τ_e, which determine the nuclear relaxation[24,26] and which are strongly modulated by the molecules' different excitation energies. A detailed study of the relaxation of our Cr(III) $S = 3/2$ and V(III) $S = 1$ compounds is beyond the scope of this paper, but as a rule of thumb, it would be difficult if not impossible to observe NMR signals of a compound that yields a well-resolved EPR spectrum at a given temperature. Surprisingly, in the case of $K_4[V(CN)_7]$ neither EPR signals could be observed,[32e] nor were we able to see ^{15}N MAS NMR signals. The $[Cr(CN)_6]^{3-}$ ion is a borderline case. On the one hand, it has been studied successfully by EPR spectroscopy even as bulk material;[35] on the other hand, it also gave the ^{15}N MAS NMR spectrum represented in Figure 6, which was

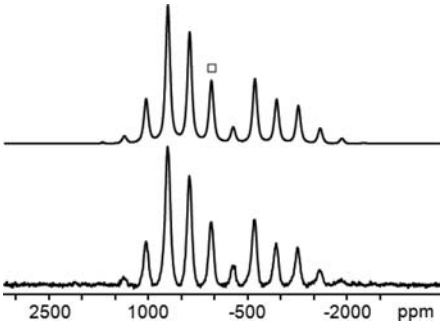

Figure 6. ^{15}N MAS NMR spectrum of $Cs_2K[Cr(CN)_6]$: bottom, experimental, ν_r = 10 kHz, T = 311.6 K; top, simulated with the data given in Table S5, Supporting Information.

obtained from $Cs_2K[Cr(CN)_6]$. The isotropic signal near 630 ppm had a signal width at half height of 2540 Hz, which is too large to resolve the different CN ligands of the slightly distorted $[Cr(CN)_6]^{3-}$ ion.

Hexacyanochromate(II). The synthesis of alkali salts of $[Cr(CN)_6]^{4-}$ has been reported to be demanding[36] because they are rather unstable in air and water owing to the low redox potential of the Cr(II) species.[37] $K_4[Cr(CN)_6]$ has been claimed to exist anhydrous or as $K_4[Cr(CN)_6](H_2O)_2$,[36b] while the dark green-blue sample studied here contained three H_2O per $K_4[Cr(CN)_6]$ according to elemental analysis. Incomplete drying of the sample could accidentally account for one water molecule in excess, or the structure could be analogous to that known for $K_4[Fe(CN)_6](H_2O)_3$.[38]

The synthesis of $K_4[Cr(CN)_6](H_2O)_3$ was repeated with KCN enriched in ^{15}N and ^{13}C, respectively, and microcrystalline samples were studied by MAS NMR spectroscopy (Figures 7 and 8). There are six isotropic ^{15}N NMR signals, which point to two different distorted $[Cr(CN)_6]^{4-}$ ions. Two signals appear around 500 ppm well separated from four others between 740 and 820 ppm. This fits well into the assignment strategy mentioned above: the signals around 500 ppm belong to the axial CN ligands and those between 740 and 820 ppm to

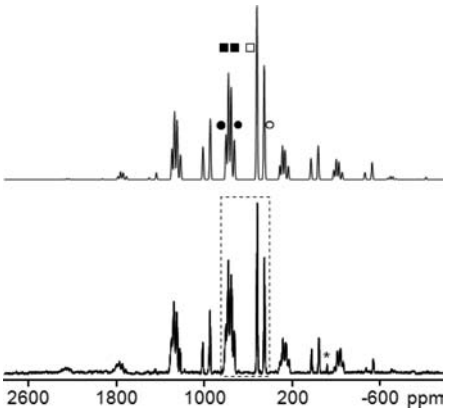

Figure 7. ^{15}N MAS NMR spectrum of $K_4[Cr(CN)_6](H_2O)_3$: bottom, experimental, ν_r = 15 kHz, T = 304.9 K; isotropic signals are framed; ∗, KCN; top, simulated with the data given in Table S5, Supporting Information. For signal assignment, see text and Figure 1.

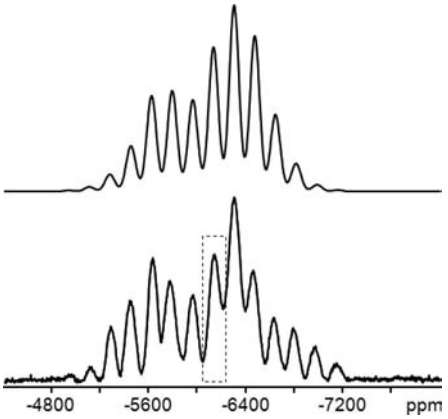

Figure 8. ^{13}C MAS NMR spectrum of $K_4[Cr(CN)_6](H_2O)_3$: bottom, experimental, ν_r = 13 kHz, T = 300.3 K; isotropic signal is framed; top, simulated with the data given in Table S5, Supporting Information.

the equatorial CN ligands. The integration of the sideband spectra of all isotropic signals suggested to assign the high- and low-intensity signals to $[Cr(CN)_6]^{4-}$ ions of two different sites in the lattice. The assignment is in part tentative because the intensities suffer from some scatter (Table S5, Supporting Information). The crystal sites will be discussed below together with the manganese analogue.

The resolution of the ^{13}C MAS NMR spectrum (Figure 8) of $K_4[Cr(CN)_6](H_2O)_3$ is not as good as that of the ^{15}N MAS NMR spectrum. There is one isotropic signal at −6140 ppm, which seems to be composed of several resonances. But signal deconvolution gave random results depending on the starting conditions. The signal overlap is also reflected in the sideband pattern the intensities of which could not be reproduced very well. This must be due to the fact that the positions and the intensities of the overlapping resonances are not known. Note that all other simulations of this work were satisfactory, in accord with better signal resolution.

Quite strikingly, $[Cr(CN)_6]^{4-}$ does give ^{13}C NMR signals, whereas $[Cr(CN)_6]^{3-}$ does not. This is useful for detecting low-spin Cr^{2+} ions in the presence of Cr^{3+} ions, and it is in accord with the electron relaxation time of Cr^{2+} ions being shorter than that of Cr^{3+} ions.[24,26] However, the spin state also plays an important role; for instance, high-spin Cr^{2+} ions in

dx.doi.org/10.1021/ic401830f | Inorg. Chem. 2013, 52, 12634−12644

octahedral and tetrahedral environments relax more slowly so that they can be detected by EPR methods.[39]

Hexacyanomanganate(II). Before turning to the synthesis of the ^{15}N- and ^{13}C-enriched derivatives, we optimized the yield by modifying the procedure of Figgis who has formulated the product as $K_4[Mn(CN)_6](H_2O)_3$.[40] While this corresponds to $K_4[Cr(CN)_6](H_2O)_3$ described above and to the known $K_4[Fe(CN)_6](H_2O)_3$,[38] the sample subjected to elemental analysis contained less crystal water than required for $K_4[Mn(CN)_6](H_2O)_3$ probably because of prolonged drying. The ^{15}N and ^{13}C MAS NMR spectra were obtained from isotopically enriched compounds, which were dried more cautiously, but they tend to lose water so that a content of n = 2−3 H_2O is realistic. As can be seen in Figure 9, there are 13

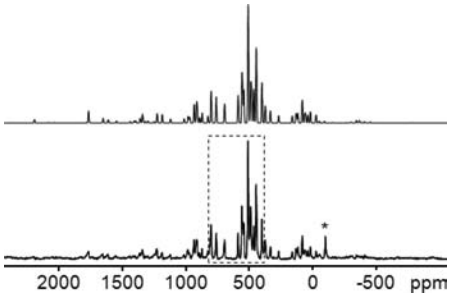

Figure 9. ^{15}N MAS NMR spectrum of $K_4[Mn(CN)_6](H_2O)_n$: bottom, experimental, ν_r = 13 kHz, T = 326.4 K; isotropic signals are framed; ∗, KCN; top, simulated with the data given in Table S6, Supporting Information. For more details, see Figure S3, Supporting Information, and text.

isotropic ^{15}N NMR signals in the range 410−810 ppm, more signals than for any other cyanometalate studied so far. Two signals appear as shoulders, which can be well-defined via deconvolution (Figure S3, Supporting Information). But further signal overlap is indicated by the fact that multiples of three signals would be expected for distorted octahedra. Based on the integration of the deconvoluted sideband spectra, groups of signals for two equatorial and one axial CN ligands per distorted $[Mn(CN)_6]^{4-}$ ion were tentatively assigned to four different crystal sites (Table S6 and Figure S3, Supporting Information).

The isotropic ^{13}C MAS NMR signals (Figure 10) were localized between −2640 and −2830 ppm. Although the resolution is not as good as for ^{15}N, the corresponding number of 13 signals could be obtained after spectrum deconvolution (Figure S4, Supporting Information). Nine of them were assigned as described for the ^{15}N NMR signals, while for the remaining ones further analysis seemed too speculative.

The different NMR signal sets establishing nonequivalent $[Cr(CN)_6]^{4-}$ and $[Mn(CN)_6]^{4-}$ ions is obviously related to their solid-state properties, which in turn give rise to crystallographically different $[M(CN)_6]^{4-}$ octahedra (called octahedra 1 to 4 in Table S6, Supporting Information). In the series $K_4[M(CN)_6](H_2O)_3$, single crystal diffraction studies seem to exist only in the case of M = Fe.[38] For interpreting the NMR results, it is therefore assumed that the analogues with M = Cr and Mn studied here behave virtually the same way. Crystals of $K_4[Fe(CN)_6](H_2O)_3$ have been reported to be monoclinic or tetragonal at room temperature, twinning is a common feature, and all properties may be observed in one crystal.[38a] There are two types of disordered water molecules,

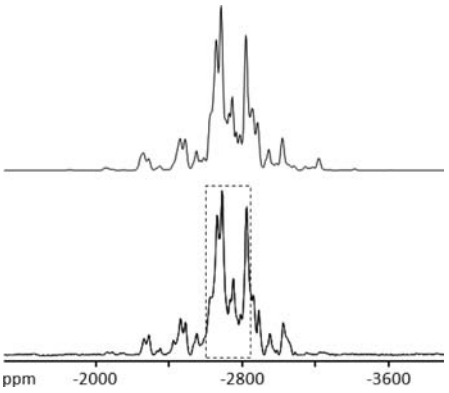

Figure 10. ^{13}C MAS NMR spectrum of $K_4[Mn(CN)_6](H_2O)_n$: bottom, experimental, ν_r = 15 kHz, T = 326.7 K; isotropic signals are framed; top, simulated with the data given in Table S6, Supporting Information. For more details, see Figure S4, Supporting Information, and text.

as established by neutron diffraction[38c] as well as by solid-state ^1H and ^2H NMR studies,[38b,41] and three different CN ligands per $[Fe(CN)_6]^{4-}$ ion have been found. In a careful study, Wasylishen[38d] has shown that even grinding of the crystals may change the structure. Clearly, these various structural features (which differ from those of $K_3[M(CN)_6]$ described above) would give rise to many ^{13}C and ^{15}N NMR signals as actually found for $K_4[Cr(CN)_6](H_2O)_3$, $K_4[Mn(CN)_6](H_2O)_n$, and the diamagnetic reference compound $K_4[Fe(CN)_6](H_2O)_3$ (Supporting Information, Experimental Section and Figures S5−S8). In some cases, the structural features could not be resolved by NMR spectroscopy. Examples already mentioned are the scatter of the signal intensities and the fact that the spectra could not always be grouped in sets of three signals expected for distorted $[M(CN)_6]^{4-}$ ions. These problems might be overcome by characterizing single crystals before grinding and investigating them by MAS NMR spectroscopy, a task that was outside the scope of this work where we were mostly interested in the spin delocalization.

Common NMR Features. The characterization of the hexacyanometalates benefits strongly from the good signal resolution as evident from the unusually large signal shifts and the relatively small signal widths. It is worth noting that this applies for undiluted solids, that is, conditions under which compounds are studied preferably by magnetic measurements. Previous NMR work dealing with the ligands of paramagnetic alkali hexacyanometalates[42] is limited to few solid-state studies and to ^{13}C giving only very broad signals.[42d] Now it turns out that detailed information is available under MAS conditions. The best nucleus is ^{15}N with a signal half width, $\Delta\nu_{1/2}(^{15}N)$, that is smaller by a factor of about 3−26 compared with $\Delta\nu_{1/2}(^{13}C)$. Here we profit by the fact that ^{15}N does not suffer from quadrupolar signal broadening like ^{14}N.[42b] Generally, the signal half width mainly depends on the electron relaxation time, τ_e, and the nuclear gyromagnetic ratio of the nucleus X, $\gamma(X)$, such that $\Delta\nu_{1/2} \propto [\gamma(X)]^2$. In the case of dipolar relaxation, it also depends on the distance r between X and the transition metal ($\Delta\nu_{1/2} \propto r^{-6}$), while in the case of contact relaxation, the spin density at the nucleus X, $\rho_s(X)$, ($\Delta\nu_{1/2} \propto [\rho_s(X)]^2$) must be considered.[24,26] The respective ratios $\Delta\nu_{1/2}(^{13}C)/\Delta\nu_{1/2}(^{15}N)$ are 6.15 for $\gamma(X)$, about 14−17 depending on r(M−C) and r(M···N) (cf. Table S1, Supporting Information) and about 15−110 for $\rho_s(X)$ of the hexacyano-

dx.doi.org/10.1021/ic401830f | Inorg. Chem. 2013, 52, 12634−12644

metalates (Tables S3−S7, Supporting Information). The latter theoretical ratios of the squared spin densities are much larger than the experimental ratios of the signal half widths, which means that dipolar rather than contact relaxation is predominant. With the numbers given above, the width of the missing ^{13}C NMR signal of $Cs_2K[Cr(CN)_6]$ can be estimated. If only the factor $[\gamma(X)]^2 = 6.15$ is applied to the width of the unresolved ^{15}N NMR signals (2540 Hz), $\Delta\nu_{1/2}(^{13}C) > 15$ kHz is expected, and this would be hard to detect by MAS NMR. If in addition the atomic distances are considered, $\Delta\nu_{1/2}(^{13}C)$ would increase to about 1.3 MHz. The most important parameter is τ_e, which proved favorable throughout except for the borderline case $[Cr(CN)_6]^{3-}$ and for $[V(CN)_7]^{4-}$.

The spinning sideband spectra are unusually large, which is a signature of anisotropic interaction between the spin source M and the CN ligand nuclei. As expected from the local symmetry at the C and N atoms (see below), the shift tensors proved to be axial or close to axial unless signal overlap interfered. This pointed to only small bulk susceptibility contributions[43] to the sideband pattern as could be expected from the relatively small magnetic volume susceptibility (3×10^{-6} to 7×10^{-6}). The deviation from axial symmetry of the shift tensors of overlapping signals decreased upon signal deconvolution. But because the procedure suffered from arbitrariness, these patterns were not considered further. Another contribution to the spectral pattern is the internuclear dipole interaction due to the nuclear and quadrupolar moments. For the ^{15}N NMR spectra, it is negligible because of the high isotopic dilution of the adjacent ^{13}C nuclei. The amount of the $^{13}C,^{14}N$ dipole−dipole coupling in the CN ligand is close to 2 kHz, that is, about 2% of the width of the pattern, and has been neglected, while most of the quadrupolar coupling is spun away.[44] Hence the spinning sidebands can be analyzed as being due to the magnetic contributions, which are discussed in the next sections.

Access to the Spin Densities. The spin density felt by a nucleus X originates from the electron−nuclear interaction and is described by the hyperfine (hf) coupling constant, $A(X)$, which in turn determines the NMR signal shift, $\delta_T(X)$, at the temperature T.[24,45] It may be expressed as the (dimensionless) fraction (of time), $f(X) \leq 1$, of the unpaired electron in the respective orbital or quoted as $\rho(X)$ in atomic units, $(au)^{-3}$. For solid samples, as studied here, two experimental parameters are of interest.[46] First, there is the isotropic shift, $\delta_{T,iso}(X)$, which is related through the isotropic hf coupling, $A_s(X)$, to the spin density in the s orbital of the ith electron shell, $|\psi_{is}(0)|^2 f_{is}(X)$:

$$A_s(X) = \frac{\mu_0}{3S} g_e \beta_e \gamma_n |\psi_{is}(0)|^2 f_{is}(X) \quad (1)$$

Second, there is the shift anisotropy, which is related through the anisotropy of the hf coupling, $\Delta A_p(X)$, to the spin density in the p orbitals of the ith electron shell, $\langle r_{ip}^{-3}\rangle f_{ip}(X)$:

$$\Delta A_p(X) = \frac{\mu_0}{8\pi S} \Delta a g_e \beta_e \gamma_n \langle r_{ip}^{-3}\rangle f_{ip}(X) \quad (2)$$

In eqs 1 and 2, μ_0 is the magnetic constant, S is the electron spin quantum number, g_e is the electron **g** factor, β_e is the Bohr magneton, and γ_n is the nuclear gyromagnetic ratio. The function ψ_{is} describing the semioccupied orbital and the spin density, $|\psi_{is}(0)|^2$ (given in Å^{-3}), refer to the ith s orbital of the nucleus, while the average of the spatial distribution of the unpaired electron, $\langle r_{ip}^{-3}\rangle$, refers to the ith p orbital. Since both are one-electron terms, the normalization factor $1/2S$ included in eqs 1 and 2 accounts for the number of unpaired electrons per molecule. Finally, the factor Δa in eq 2 accounts for the axially symmetric case, that is, the orientation of a p orbital in the local axis system. In the following, f_i will be called fractional spin density and the label for the nucleus X in eqs 1 and 2 will be dropped for convenience; it shall be reintroduced below when proceeding to specific results.

The isotropic and anisotropic hyperfine interactions are related to the corresponding components of the chemical shift tensor,[47] which can be determined from the MAS NMR spectrum[48] by spinning sideband analysis.[49] The analysis provides the experimental isotropic shift, $\delta^{exp}_{T,iso} = (\delta^{exp}_{T,ZZ} + \delta^{exp}_{T,XX} + \delta^{exp}_{T,YY})/3$, with the principal components of the chemical shift tensor, δ_{ZZ}, δ_{XX}, and δ_{YY} (ordered as $|\delta^{exp}_{T,ZZ} - \delta^{exp}_{T,iso}| \geq |\delta^{exp}_{T,XX} - \delta^{exp}_{T,iso}| \geq |\delta^{exp}_{T,YY} - \delta^{exp}_{T,iso}|$). Further common parameters of characterization are the anisotropy, $\Delta\delta^{exp}_T = \delta^{exp}_{T,ZZ} - (\delta^{exp}_{T,XX} + \delta^{exp}_{T,YY})/2$, and the asymmetry, $\eta^{exp}_T = (\delta^{exp}_{T,YY} - \delta^{exp}_{T,XX})/(\delta^{exp}_{T,ZZ} - \delta^{exp}_{T,iso})$.[50] The hyperfine coupling constants of eqs 1 and 2 are related to the through-bond or contact part of the electron−nuclear interaction, and for a powder this is given by

$$\delta^{con}_T = \delta^{con}_{T,iso} + \frac{1}{2}\Delta\delta^{con}_T(3\cos^2\chi - 1) \quad (3)$$

where $\delta^{con}_{T,iso}$ is the isotropic contact shift. The second term represents the anisotropy where χ is the angle that the principal axis system of the tensor can adopt relative to the external field.

Isotropic Spin Density. The isotropic hyperfine coupling due to the through-bond interaction is obtained from the isotropic NMR signal shift by[51]

$$\delta^{con}_{T,iso} = \frac{g_e\beta_e S(S+1)}{3\gamma_n k_B T} A_s F(g_{ii}, D) \quad (4)$$

where k_B is the Boltzmann factor, T is the absolute temperature, and $F(g_{ii},D)$ is a function of the components g_{ii} of the **g** tensor and the zero-field splitting D. In the case of $S = 1/2$, one gets $F(g_{ii},D) = 1$, while for the hexacyanometalates with $S > 1/2$, the **g** tensor is often virtually isotropic so that the function is negligibly small. After combining eqs 1 and 4, the dimensionless fractional spin density in the ith s orbital of a $S = 1/2$ compound is derived from the contact shift by

$$f_{is} = \frac{9k_BT}{\mu_0 g_e^2 \beta_e^2 (S+1)|\psi_{is}(0)|^2}\delta^{con}_{T,iso} = 3.426 \times 10^{-4}\frac{\delta^{con}_{298,iso}}{g_{av}^2(S+1)|\psi_{is}(0)|^2} \quad (5)$$

In eq 5, the respective constants[52] and the standard temperature 298 K have been inserted, g_e has been replaced by the average experimental **g** factor, g_{av}, and the shift (at 298 K) is given in ppm. It is worth noting that f_{is} depends on the wave function $\psi_{is}(0)$, which should be known for the compound under study. Alternatively, and preferred in this work, the fractional spin density may be given in atomic units, $(au)^{-3}$. It is then often cited as $\rho(X)$.

$$\rho_{is}(X) = \frac{9k_BTa_0^3}{\mu_0 g_{av}^2 \beta_e^2 (S+1)|\psi_{is}(0)|^2}\delta^{con}_{T,iso} = 5.077 \times 10^{-5}\frac{\delta^{con}_{298,iso}}{g_{av}^2(S+1)|\psi_{is}(0)|^2} \quad (6)$$

dx.doi.org/10.1021/ic401830f | Inorg. Chem. 2013, 52, 12634−12644

In order to obtain $\delta^{con}_{298,iso}$ values, the experimental isotropic shifts, $\delta^{exp}_{T,iso}$, must be corrected as indicated by eq 7.

$$\delta^{con}_{298,iso} = (\delta^{exp}_{T,iso} - \delta^{dia}_{iso} - \delta^{dip}_{T,iso})T/298 \quad (7)$$

Here δ^{dia}_{iso} is the shift the signal would have if the compound were diamagnetic, and $\delta^{dip}_{T,iso}$ is the shift due to the through-space (or dipolar) effect of the unpaired electrons on the nucleus. It follows from eq 7 that each paramagnetic signal has its own reference signal. For spectra consisting of several signals, this would entail several δ^{con} scales, and therefore, they are usually represented relative to references like TMS for ^{13}C and CH_3NO_2 for ^{15}N as in this work. By application of eq 7, some errors may be introduced which, as will turn out, are usually small compared with the large overall signal shifts. Thus, for δ^{dia}_{iso}, the ^{13}C and ^{15}N MAS NMR spectra of the corresponding diamagnetic compounds $K_4[Fe(CN)_6](H_2O)_3$ (Figures S5−S8, Supporting Information) and $Cs_2K[Co(CN)_6]$ were recorded (Supporting Information, Experimental Section and Figures S5−S8 and S9 and S10). Their signal shifts may differ by several ppm from the genuine diamagnetic (or orbital) contribution.[27] In addition, in the spectra of $K_4[Fe(CN)_6](H_2O)_3$, the signals arising from the structural diversity mentioned above could not be assigned. Therefore, a mean diamagnetic reference shift was applied entailing an error of up to about 10 ppm or <0.5%. For the temperature scaling, it was assumed that δ^{dia}_{iso} is temperature independent as usual and that in the case of $\delta^{exp}_{T,iso}$ and δ^{dip}_{T} the Curie law is valid. Since the spectra were recorded close to the standard temperature, 298 K, the potential error is small. The conventional calculation of the dipolar shifts follows eq 8,[45,51]

$$\delta^{dip}_{T} = \frac{\mu_0}{4\pi}\frac{\beta_e^2 S(S+1)}{9k_B T}\sum_j \frac{3\cos^2\theta_j - 1}{r_j^3} F'(g_{ii}, D) \quad (8)$$

where r_j are the vectors joining the respective ligand atom and the paramagnetic centers of the lattice, θ_j are the angles between r_j and the principal magnetic axis of the molecule, and $F'(g_{ii},D)$ is a function (different from that in eq 4) of the components g_{ii} of the **g** tensor and of the zero-field splitting D. Equation 8 had originally been derived for solutions, but it is also valid for the solid state.[53] Since the **g** tensors are almost isotropic, the dipolar shifts are negligibly small. Exceptions are the ion $[Fe(CN)_6]^{3-}$ with $\delta^{dip}_{T,iso}(^{13}C)$ and $\delta^{dip}_{T,iso}(^{15}N)$ up to 2% and 1%, respectively, of the total shift, as well as the ion $[Mn(CN)_6]^{4-}$ with $\delta^{dip}_{T,iso}(^{13}C)$ and $\delta^{dip}_{T,iso}(^{15}N)$ up to 10% and 7%, respectively. It must be noted however that the **g** factors result from low-temperature experiments, while in this study, the NMR data were obtained at ambient temperature. Actually, the **g** factors may change with the temperature owing to, for instance, the spin population of higher states and phase transitions. An example is $K_3[Fe(CN)_6]$ whose **g** factor anisotropy is much smaller at 100 K than at 20 K.[33,54] Likewise, with the **g** factors given for $Cs_2K[Fe(CN)_6]$,[55] the dipolar shifts differ by >10%. The parameters used for calculating the dipolar shifts are collected in Table S1 and the resulting values in Table S2, Supporting Information. In some cases, it was not possible to fully assign the signals so that the application of eq 7 to axial and equatorial CN ligands was not meaningful. In these cases, only the paramagnetic shifts, $\delta^{para}_{T,ii}$ and $\delta^{para}_{T,iso}$, are given.

The contact shifts obtained with eq 7 were converted to the spin densities by way of eqs 5 and 6. The details are listed in the Supporting Information, Tables S3−S7, while a summary is given in Figure 11. The fractional spin densities of eq 5 are given in percent for the average total spin at the ligand C and N

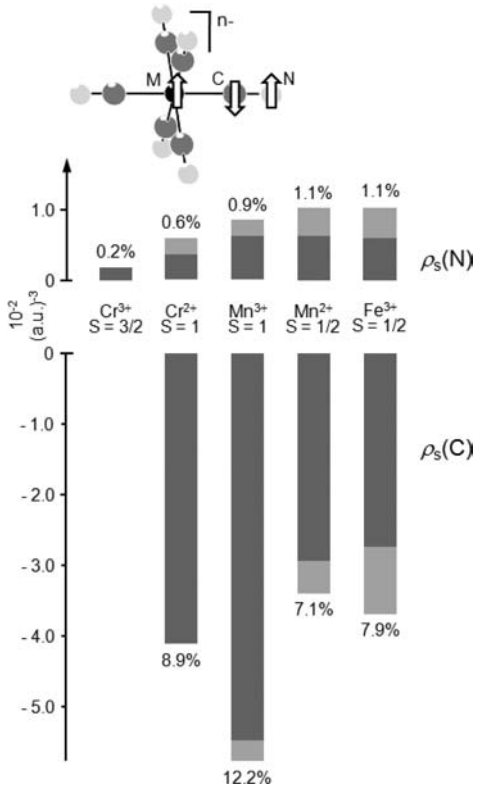

Figure 11. Transfer of isotropic spin density to and induction in ligand orbitals of the hexacyanometalates $[M(CN)_6]^{n-}$ with M = Cr^{3+}, Cr^{2+}, Mn^{3+}, Mn^{2+}, and Fe^{3+}: top, spin signs in the M−C−N fragments; bottom, maximal amount of the spin densities ρ_{2s}(C) and ρ_{2s}(N) per CN ligand (dark gray bars) and scatter of the spin densities (light gray bars). The fractional spin densities are given in % for a set of six ligands.

atoms of $[M(CN)_6]^{n-}$. They depend on the wave function used for the calculation of $|\psi_{is}(0)|^2$.[56] For an estimate, those of ref 56b were employed, and it was assumed that the spin is in the valence s orbital. We cannot exclude the involvement of 1s orbitals (through cross terms with 2s orbitals),[46,57] but this does not affect the following general conclusions. It turns out that all compounds have negative spin density in the 2s orbital of the C atoms, while at the N atoms the spin is positive. This is in line with the fact that the hexacyanometalates studied have no unpaired electrons in d_σ (e_g) orbitals (apart from little spin due to polarization, see below) and that a singly occupied d_π (t_{2g}) orbital interacts with the ligand π and π^* orbitals such that the MO coefficient at C is small while at N it is big. Actually, the positive spin at C is so small that it is largely overcompensated by negative spin resulting from electron exchange interaction in the M−C and (less so) the C−N bonds. As a result, spin polarization is dominating, which has been discussed for cyanometalates previously.[19,58] Remarkably, the average amount of spin is larger at the carbon atoms than at the nitrogen atoms (ranging from a factor of 7.4 for $[Fe(CN)_6]^{3-}$ up to 14.0 for $[Cr(CN)_6]^{4-}$ for spin fractions), while both spin delocalization and induction reach a maximum for $[Mn(CN)_6]^{3-}$. The spin density at C and N varies considerably as indicated by the light gray subareas of the bars in Figure 11. This can be understood as structure-induced

dx.doi.org/10.1021/ic401830f | Inorg. Chem. 2013, 52, 12634−12644

disorder of the spin densities, a phenomenon that is expected to have an impact on the magnetic ordering[5,59] and photomagnetic switching[11−14] occurring in Prussian blue-type materials.

The relative resolution of spin densities is unusually high; for example, it is higher than $\pm 2 \times 10^{-4}$ (au)$^{-3}$ for $[Mn(CN)_6]^{4-}$, while for absolute values it would be somewhat lower because of the small errors mentioned above. The NMR resolution is related to the more general issue of nonequivalent atoms or ions in the crystal lattice, which is usually probed by X-ray crystal analysis. It is also of interest for the Jahn−Teller distortion of the hexacyanometalates.[60] For instance, the mean scaled spread of the isotropic ^{15}N NMR signals (spread/average of $\delta^{exp}_{T,iso}$) increases in the series $Cs_2K[Fe(CN)_6]$ (3.2%), $Cs_2K[Mn(CN)_6]$ (13.4%), and $K_4[Mn(CN)_6]$ (39.5%). This confirms the calculated trend of distortions, which may however be partly due to the different crystal packing.[60b]

Anisotropic Features. Because the spectra of the $[M(CN)_6]^{n-}$ ions in Figures 1−4 and 6−10 show large sideband patterns, the interaction between the metal and the CN ligands must have an anisotropic contribution. When the anisotropy is dominated by the Fermi contact interaction, part of the spin density would therefore be in MOs to which carbon and nitrogen p AOs are admixed, and this would corroborate the bonding model.[19,58] As indicated by eqs 2 and 3, the shift anisotropy, $\Delta\delta^{con}_T$, is related to the fractional anisotropic spin density, f_{ip}, in the ith p orbital. For axial shift tensors, it is given by $\Delta\delta^{con}_T = \delta^{con}_{T,\parallel} - \delta^{con}_{T,\perp}$ where $\delta^{con}_{T,\parallel}$ and $\delta^{con}_{T,\perp}$ are the respective components parallel and perpendicular to the principal axis. The treatment of the hexacyanometalates follows that of the metallocenes.[48e] It can be simplified by considering cases where the **g**-factor anisotropy is small so that the averaged magnetic moment is aligned along the external field and by disregarding small deviations of the M−C−N fragments from local axial symmetry. Note that the site symmetry of the ligand C and N atoms of the $[M(CN)_6]^{n-}$ ions in the crystal is low, but the experimental shift tensors are axial or close to axial unless signal overlap prevents proper analysis. Then the principal values of the nuclear shift tensors are parallel to the axes of the $[M(CN)_6]^{n-}$ octahedra and $\delta^{con}_{T,\parallel}$ is aligned along the M−C−N bond being defined as the z direction.

The experimental shift anisotropy at the temperature T, $\Delta\delta^{exp}_T = \delta^{exp}_{T,\parallel} - \delta^{exp}_{T,\perp}$, has diamagnetic and paramagnetic contributions, $\Delta\delta^{dia}$ and $\Delta\delta^{para}_T$, respectively. The latter is the sum of the contact term, $\Delta\delta^{con}_T$, and the dipolar term, $\Delta\delta^{dip}_T$:

$$\Delta\delta^{exp}_T = \Delta\delta^{para}_T + \Delta\delta^{dia} = \Delta\delta^{con}_T + \Delta\delta^{dip}_T + \Delta\delta^{dia}. \quad (9)$$

In a powder, these contributions depend on the variable angle, χ, that the molecular z axis can adopt relative to the applied field $\mathbf{B}_0$ (Figure 12). They are described as follows.[48a,e]

(i) The contact contribution, $\Delta\delta^{con}_T(\chi)$, reflecting the spin density in the $2p_i$ orbital of the nucleus X is given by

$$\Delta\delta^{con}_T(X) = C\Delta a\langle r_{X,2p}{}^{-3}\rangle f_{2p_i}(X)\frac{1}{2}(3\cos^2\chi - 1) \quad \text{with}$$

$$C = \frac{\mu_0}{4\pi}\frac{g_{av}{}^2\beta_e{}^2 S(S+1)}{3k_BT} \quad (10)$$

The orientation of the p_i orbital is considered by the tensor anisotropy $\Delta a = a_\parallel - a_\perp$ with the principal values along the M−C−N bond ($a_\parallel = 4/5$) and perpendicular to it ($a_\perp = -2/5$).[56a] Then, in the case of p_σ and p_π orbitals, Δa becomes 6/5 and −3/5, respectively.

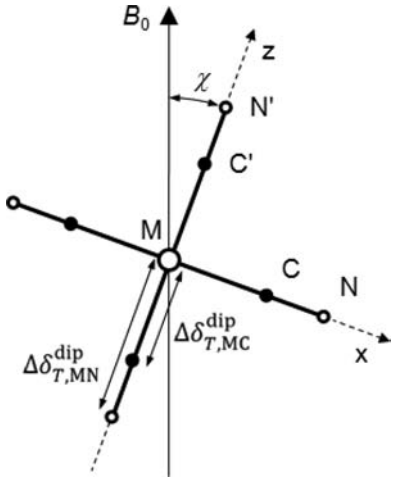

Figure 12. View on $[M(CN)_6]^{n-}$ down the atom sequence NCMCN in the y direction showing selected interactions leading to dipolar shifts in $[M(CN)_6]^{n-}$ ions (see text).

(ii) The dipolar shift, $\Delta\delta^{dip}_T(X)$, includes the through-space interaction between the observed nucleus and all paramagnetic centers in the crystal lattice. Because it decreases rapidly with the distance (see eq 11 below), the $[M(CN)_6]^{n-}$ ions can be regarded as being isolated. We are thus left with the interactions $\Delta\delta^{dip}_T(X)$ between the atom pairs shown in Figure 12.When an isolated CN ligand is considered, the dipolar contribution experienced by the atom X due to spin in the orbitals of the metal M is described by

$$\Delta\delta^{dip}_{T,MX}(X) = Cr_{M-X}{}^{-3}(1 - 6f_{2p_i}(N))\frac{1}{2}(3\cos^2\chi - 1) \quad (11)$$

where r_{M-X} is the distance between the metal and the atom X = C or N. The spin density at the ion M^{n+} is diminished by the fractions $f_{2p_i}(N)$ delocalized to the six ligand N atoms.

(iii) The remaining diamagnetic contribution

$$\Delta\delta^{dia}(X) = \Delta\delta^{dia}\frac{1}{2}(3\cos^2\chi - 1) \quad (13)$$

can be approximated by the shift anisotropy, $\Delta\delta^{dia}$, measured for an isostructural diamagnetic hexacyanometalate. Considering that the angular dependent factor in eqs 10−13 is the same as that of the experimental shift anisotropy, inserting eqs 10−13 into eq 9 and solving for the fractional anisotropic spin density in the respective 2p orbitals yields

$$f_{2p_i}(N) = \frac{\frac{\Delta\delta^{para}_T(N)}{C} - r_{M-N}{}^{-3}}{(\Delta a\langle r_{N,2p}{}^{-3}\rangle - 6r_{M-N}{}^{-3})} \quad (14)$$

$$f_{2p_i}(C) = \frac{\frac{\Delta\delta^{para}_T(C)}{C} - r_{M-C}{}^{-3} + f_{2p_i}(N)6r_{M-C}{}^{-3}}{\Delta a\langle r_{C,2p}{}^{-3}\rangle} \quad (15)$$

For the NMR data in ppm and at the standard temperature 298 K, the constant is $C = 697 g_{av}{}^2 S(S+1)$ Å^3.

Estimation of the spin densities at the CN ligand by using eqs 14 and 15 yields the data of all compounds in Table S8, Supporting Information. Two representative examples, the axial CN ligands of $K_4[Cr(CN)_6]$ and $Cs_2K[Fe(CN)_6]$, are visualized in Figure 13. The assignment is along ($2p_\sigma$) and perpendicular ($2p_\pi$) to the M−C−N direction.

dx.doi.org/10.1021/ic401830f | Inorg. Chem. 2013, 52, 12634−12644

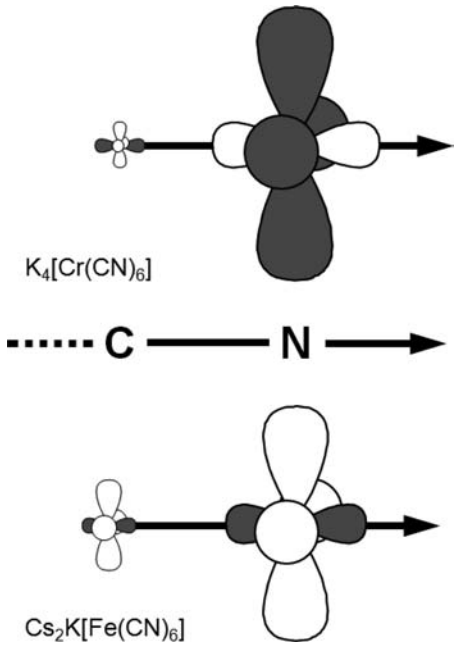

Figure 13. Spin densities at the axial CN ligands of selected hexacyanometalates. Qualitative representation of the data in Table S8, Supporting Information, dark and light components represent positive and negative spin, respectively; the arrow designates the local principal axis.

Evidently, much spin is transferred from the metal to the π orbitals of the N atoms, and only a small amount is found at those of the C atoms. This is in accord with the bonding model.[19,58] In addition, spin appears along the M−C−N σ bonds, which complements the spin in the s orbitals (see previous section). The π spin at the N atoms of $K_4[Cr(CN)_6]$ and $Cs_2K[Cr(CN)_6]$ is negative as expected and as found in the PND study[22] of $Cs_2K[Cr(CN)_6]$ (see next section). However, on passing to $Cs_2K[Fe(CN)_6]$ and $Cs_2K[Mn(CN)_6]$, the π spin becomes positive. This follows cogently from the sign of the shift anisotropy whose change is easily inferred from the inverted shapes of the ^{15}N spinning sideband manifolds of, for example, $Cs_2K[Cr(CN)_6]$ (Figure 8) and $K_3[Mn(CN)_6]$ (Figure 1) or, more clearly, $Cs_2K[Mn(CN)_6]$ (Figure 1 of ref 25). The σ spin at the N atoms of $K_4[Cr(CN)_6]$ and $Cs_2K[Cr(CN)_6]$ is negative, again in accord with the PND results of $Cs_2K[Cr(CN)_6]$, but it is positive for $Cs_2K[Fe(CN)_6]$ and $Cs_2K[Mn(CN)_6]$. The change of the spin sign deserves further studies.

Comparison with Other Methods. Several groups have joined forces to carry out elaborate PND studies on $Cs_2K[Fe(CN)_6]$[21] and $Cs_2K[Cr(CN)_6]$.[22] By use of many-parameter fits of the diffraction data, the results listed in Table 1 were obtained. As mentioned above, in the case of $Cs_2K[Cr(CN)_6]$, the spin signs are in accord with our NMR results, and beyond that, the numerical agreement is acceptable. The PND method does not distinguish between spin in the $2p_z$ and 2s orbitals, while the NMR method does. On the other hand, different lobes of the $2p_z$ orbitals are visible by PND and not by NMR.

Unfortunately, the anisotropy of the spin density at the N atoms of $Cs_2K[Fe(CN)_6]$ could not be obtained from the PND studies, so there is no independent proof of the sign of its π component seen by NMR. The PND data are less precise than those of $Cs_2K[Cr(CN)_6]$ because there are two unpaired electrons less than for the chromium analogue. Note also that for $Cs_2K[Fe(CN)_6]$, fractions of the magnetization are obtained rather than spin densities because both spin and orbital moments must be considered.[21b] Since the separation of these contributions is difficult, the overall magnetization distribution and not just the spin distribution is determined. In the NMR approach, the effect of the angular moment is covered by the dipolar signal shift, which may be calculated[51] and eliminated so that contact shifts remain and spin densities are available. Besides, the results of PND and NMR studies are expected to be different when excited states are thermally accessible because PND studies are carried out near 4 K while MAS NMR spectra are usually recorded near 300 K. Slightly different magnetization densities ascribed to two nonequivalent ions in the asymmetric unit of $Cs_2K[Fe(CN)_6]$ have been reported.[21c] These could not be resolved by MAS NMR spectroscopy.

The EPR support of the present NMR results is very limited owing to the relaxation constraints discussed above. The only example seems to be Cr^{3+} in $Cs_2Li[Co(CN)_6]$.[61] The amount of the spin density in the nitrogen 2s orbitals is close to that found by NMR (Table 1), but the sign was not determined experimentally.

■ CONCLUSIONS

MAS NMR spectroscopy of microcrystalline hexacyanometalates yields detailed information on the delocalization of unpaired spin from the metal center to the carbon and nitrogen atoms of the CN ligands. Most of the $[M(CN)_6]^{n-}$ ions have sufficiently short electron relaxation times so that, despite short distances between the spin center and the investigated ligand nuclei, high signal resolution is achieved. Generally, the more distant N atoms yield better resolved spectra. There may be borderline cases such as $[Cr(CN)_6]^{3-}$ where only nitrogen can be detected. In order to obtain good-quality spectra with standard equipment and in acceptable recording times isotopic

Table 1. Spin Densities[a] Obtained from NMR, PND, and EPR for the 2s, $2p_\sigma$, and $2p_\pi$ Ligand Orbitals of Hexacyanometalates

compound	S	atom	method	ref	f_{2s}	$f_{2p_z}+f_{2s}$	f_{2p_π}	$\sum f^b$
$[Cr(CN)_6]^{3-}$	3/2	N	NMR[c]	this work	0.0004	−0.014	0.055	
			PND	22a		−0.011[d]	0.029	
			EPR	61	±0.0003			
$[Fe(CN)_6]^{3-}$	1/2	C	NMR[c]	this work	−0.013	−0.006	−0.027	
			PND	21c				−0.008
		N	NMR[c]	this work	0.002	0.015	−0.052	
			PND	21c				0.010

[a]Given as fraction per atom and per unpaired electron. [b]Overall magnetization per atom as a measure of the overall spin density. [c]Weighted mean of axial and equatorial ligands. [d]Sum of the component along the N−C bond and the lone pair.

dx.doi.org/10.1021/ic401830f | Inorg. Chem. 2013, 52, 12634−12644

enrichment is advisable. Proper spectrum analysis may require high spinning frequencies.

The spin density can be assigned to the 2s, $2p_\sigma$, and $2p_\pi$ orbitals of the ligand atoms. The 2s spin density ranges from 7% to 12% for a set of six C atoms and 0.2% to 1.1% for a set of six N atoms, all compared with the spin originally localized at the respective metal. From the signs of these spin densities, it follows that they are induced through polarization of the M−C and C−N bonds. Moreover, direct spin delocalization within the singly occupied π-type MOs can be studied. It is most important for the N atoms and nonzero, albeit small, for the C atoms. According to the $2p_\sigma$ data some spin is also found along the M−C−N bonds including the lobes corresponding to the lone pairs at the N atoms. The study uncovers distortions of the $[M(CN)_6]^{n-}$ ions, and, in most cases, strong crystal disorder, which is accompanied by a spread of spin densities.

The average amount of the local spin density, its scatter, its sign, and its orientation merits attention for the design and the de facto properties of cyanide-bridged magnetic materials.

■ ASSOCIATED CONTENT

Ⓢ Supporting Information

Experimental procedures, NMR spectra of $K_3[Mn(CN)_6]$, $K_3[Fe(CN)_6]$, $K_4[Mn(CN)_6](H_2O)_n$, $K_4[Fe(CN)_6](H_2O)_3$, and $Cs_2K[Co(CN)_6]$, calculation of the isotropic dipolar shifts, and tables of the solid-state ^{13}C NMR data, ^{15}N NMR data, isotropic spin densities, and spin in the p orbitals of all paramagnetic hexacyanometalates. This material is available free of charge via the Internet at http://pubs.acs.org.

■ AUTHOR INFORMATION

Corresponding Author

*E-mail: f.h.koehler@lrz.tu-muenchen.de.

Notes

The authors declare no competing financial interest.

■ ACKNOWLEDGMENTS

This work was supported by the Deutsche Forschungsgemeinschaft, Priority Program 1137 entitled “Molecular Magnetism” (2002−2007), and was in part supported by the Bayerisch-Französisches Hochschulzentrum.

■ REFERENCES

(1) (a) Ferlay, S.; Mallah, T.; Quahès, R.; Veillet, P.; Verdaguer, M. *Nature* **1995**, *378*, 701−703. (b) Holmes, S. M.; Girolami, G. S. *J. Am. Chem. Soc.* **1999**, *121*, 5593−5594. (c) Hatlevik, O.; Buschmann, W. E.; Zhang, J.; Mamson, J.; Miller, J. S. *Adv. Mater.* **1999**, *11*, 914−918.

(2) (a) Pilkington, M.; Decurtins, S. In *Comprehensive Coordination Chemistry II*; McCleverty, J. A., Meyer, T. J. Eds.; Elsevier: Oxford, 2004; Vol. 7, pp 177−226. (b) Rebilly, J.-N.; Mallah, T. *Struct. Bonding (Berlin)* **2006**, *122*, 102−133.

(3) Beltran, M. L. C.; Long, J. R. *Acc. Chem. Res.* **2005**, *38*, 325−334.

(4) Lescouëzec, R.; Toma, L. M.; Vaissermann, J. M.; Verdaguer, M.; Delgado, F. S.; Ruiz-Perez, C.; Lloret, F.; Julve, M. *Coord. Chem. Rev.* **2005**, *247*, 2691−2729.

(5) Verdaguer, M.; Girolami, G. *Magnetism: Molecules to Materials V*; Miller, J. S., Drillon, M. Eds.; Wiley-VCH: Weinheim, Germany, 2005; Vol. 5, pp 283−346.

(6) Newton, G. N.; Nihei, M.; Oshio, H. *Eur. J. Inorg. Chem.* **2011**, 3031−3042.

(7) (a) Schelter, E. J.; Prosvirin, A. V.; Dunbar, K. R. *J. Am. Chem. Soc.* **2004**, *126*, 15004−15005. (b) Li, D.; Parkin, S.; Wang, G.; Yee, G. T.; Clérac, R.; Wernsdorfer, W.; Holmes, S. M. *J. Am. Chem. Soc.* **2006**, *128*, 4214−4215. (c) Schelter, E. J.; Karadas, F.; Avendano, C.; Prosvirin, A. V.; Wernsdorfer, W.; Dunbar, K. R. *J. Am. Chem. Soc.* **2007**, *129*, 8139−8149. (d) Gu, Z.-G.; Yang, Q.-F.; Zhou, X.-H.; Zuo, J.-L.; You, X.-Z. *Inorg. Chem.* **2007**, *46*, 3236−3244. (e) Nihei, M.; Ui, M.; Hoshino, N.; Oshio, H. *Inorg. Chem.* **2008**, *47*, 6106−6108.

(8) Catala, L.; Gacoin, T.; Boilot, J.-P.; Rivière, E.; Paulsen, C.; Lhotel, E.; Mallah, T. *Adv. Mater.* **2003**, *15*, 826−829.

(9) (a) Oshio, H.; Onodera, H.; Ito, T. *Chem.—Eur. J.* **2003**, *9*, 3946−3950. (b) Nihei, M.; Ui, M.; Yokota, M.; Han, L.; Maeda, A.; Kishida, H.; Okamoto, H.; Oshio, H. *Angew. Chem., Int. Ed.* **2005**, *44*, 6484−6487. (c) Boldog, I.; Muñoz-Lara, F. J.; Gaspar, B. A.; Muñoz, M. C.; Seredyuk, M.; Real, J. A. *Inorg. Chem.* **2009**, *48*, 3710−2719. (d) Mondal, A.; Li, Y.; Seuleiman, M.; Julve, M.; Toupet, L.; Bouron-Le Cointe, M.; Lescouëzec, R. *J. Am. Chem. Soc.* **2013**, *135*, 1653−1656.

(10) Harris, D. T.; Long, J. R. *J. Chem. Soc., Chem. Commun.* **2007**, 1360−1362.

(11) Bleuzen, A.; Escax, V.; Alban, V.; Villain, F.; Verdaguer, M.; Itie, J.-P. *Angew. Chem., Int. Ed.* **2004**, *43*, 3728−3731.

(12) Mathonière, C.; Podgajny, R.; Guionneau, P.; Labrugère, C.; Sieglucka, B. *Chem. Mater.* **2005**, *17*, 442−449.

(13) Hozumi, T.; Hashimoto, K.; Ohkoshi, S. *J. Am. Chem. Soc.* **2005**, *127*, 3864−3869.

(14) Ohkoshi, S.; Tokoro, H.; Hashimoto, K. *Coord. Chem. Rev.* **2005**, *249*, 1830−1840.

(15) (a) Ruiz, E.; Rajaraman, G.; Alvarez, S.; Gillon, B.; Stride, J.; Clérac, R.; Larionova, J.; Decurtins, S. *Angew. Chem., Int. Ed.* **2005**, *44*, 2711−2715. (b) Glaser, T.; Heidemeier, M.; Weyhermüller, T.; Hoffmann, R.-D.; Rupp, H.; Müller, P. *Angew. Chem., Int. Ed.* **2006**, *45*, 6033−6037.

(16) (a) Ferbinteanu, M.; Miyasake, H.; Wernsdorfer, W.; Nakata, K.; Sugiura, K.; Yamashita, M.; Coulon, C.; Clérac, R. *J. Am. Chem. Soc.* **2005**, *127*, 3090−3099. (b) Toma, L. M.; Lescouëzec, R.; Pasán, J.; Ruiz-Perez, C.; Vaissermann, J.; Cano, J.; Carrasco, R.; Wernsdorfer, W.; Lloret, F.; Julve, M. *J. Am. Chem. Soc.* **2006**, *128*, 4842−4853.

(17) Muñoz, M. C.; Real, J. A. *Coord. Chem. Rev.* **2011**, *255*, 2068−2093.

(18) (a) Ohkoshi, S.; Tokoro, H.; Matsuda, T.; Takahashi, H.; Irie, H.; Hashimoto, K. *Angew. Chem., Int. Ed.* **2007**, *46*, 3238−3241. (b) Wang, C.-F.; Gu, Z.-G.; Lu, X.-M.; Zuo, J.-L.; You, X.-Z. *Inorg. Chem.* **2008**, *47*, 7957−7959. (c) Wen, H.-R.; Tang, Y.-Z.; Liu, C.-M.; Chen, J.-L.; Yu, C.-L. *Inorg. Chem.* **2009**, *48*, 10177−10185. (d) Wang, C.-F.; Li, D.-P.; Chen, X.; Li, X.-M.; Li, Y.-Z.; Zuo, J.-L.; You, X.-Z. *Chem. Soc., Chem. Commun.* **2009**, 6940−6942.

(19) Cano, J.; Ruiz, E.; Alvarez, S.; Verdaguer, M. *Comments Inorg. Chem.* **1998**, *20*, 27−56.

(20) (a) Tengstedt, C.; de Jong, M. P.; Kanciurzewska, A.; Carlegrim, E.; Fahlmann, M. *Phys. Rev. Lett.* **2006**, *96*, No. 057209. (b) Train, C.; Baudelet, F.; Cartier dit Moulin, C. *J. Phys. Chem. B* **2004**, *108*, 12413−12417. (c) Champion, G.; Lalioti, N.; Tangoulis, V.; Arrio, M.-A.; Sainctavit, P.; Villain, F.; Caneschi, A.; Gatteschi, D.; Giorgetti, C.; Baudelet, F.; Verdaguer, M.; Cartier dit Moulin, C. *J. Am. Chem. Soc.* **2003**, *125*, 8371−8376. (d) Champion, G.; Escax, V.; Cartier dit Moulin, C.; Bleuzen, A.; Villain, F.; Baudelet, F.; Dartyge, E.; Verdaguer, M. *J. Am. Chem. Soc.* **2001**, *123*, 12544−12546.

(21) (a) Brown, P. J.; Fischer, P.; Güdel, H. U.; Herren, F.; Ludi, A. *J. Phys. C* **1982**, *43*, 235−240. (b) Daul, C. A.; Day, P.; Figgis, B. N.; Güdel, H. U.; Herren, F.; Ludi, A.; Reynolds, P. A. *Proc. R. Soc. London, Ser. A* **1988**, *419*, 205−219. (c) Day, P.; Delfs, C. D.; Figgis, B. N.; Reynolds, P. A.; Tasset, F. *Mol. Phys.* **1993**, *78*, 769−780.

(22) (a) Figgis, B. N.; Forsyth, J. B.; Reynolds, P. A. *Inorg. Chem.* **1987**, *26*, 101−105. (b) Figgis, B. N.; Kucharski, E. S.; Vrtis, M. *J. Am. Chem. Soc.* **1993**, *115*, 176−181.

(23) Stride, J. A.; Gillon, B.; Goukassov, A.; Larionova, J.; Clérac, R.; Kahn, O. *C. R. Acad. Sci., Ser. IIc: Chim.* **2001**, *4*, 105−112.

(24) Köhler, F. H. *Magnetism: Molecules to Materials*; Miller, J. S., Drillon, M., Eds.; Wiley-VCH: Weinheim, Germany, 2001; Vol. *1*, Chapter 12.

(25) Köhler, F. H.; Lescouëzec, R. *Angew. Chem., Int. Ed.* **2004**, *43*, 2571−2573.

(26) (a) Pilbrow, J. R. *Transition Ion Electron Paramagnetic Resonance*; Clarendon Press: Oxford, U.K., 1990; Chapter 8. (b) Banci, L. In *NMR of Paramagnetic Molecules*; Berliner, L. J., Reuben, J., Eds.; Plenum Press: New York, 1993; Chapter 2. (c) Bertini, I.;Martini, G.; Luchinat, C. In *Handbook of Electron Spin Resonance*; Poole, C. P., Jr., Farach, H. A., Eds.; AIP Press: New York, 1994; Chapter 3.
(27) Kaupp, M.; Köhler, F. H. *Coord. Chem. Rev.* **2009**, *253*, 2376–2386.
(28) (a) Jagner, S.; Ljungström, E.; Vannerberg, N.-G. *Acta Chem. Scand., Ser. A* **1974**, *28*, 623–630. (b) Figgis, B. N.; Reynolds, P. A.; Williams, G. A. *Acta Crystallogr.* **1981**, *B37*, 504–508.
(29) (a) Vannerberg, N.-G. *Acta Chem. Scand.* **1970**, *24*, 2335–2348. (b) Gupta, M. P.; Milledge, H. J.; McCarthy, A. E. *Acta Crystallogr.* **1974**, *B30*, 656–661.
(30) (a) Figgis, B. N.; Gerloch, M.; Mason, R. *Proc. R. Soc. London, Ser. A* **1969**, *309*, 91–118. (b) Figgis, B. N.; Skelton, B. W.; White, A. H. *Aust. J. Chem.* **1978**, *31*, 1195–1199. (c) Morioka, Y.; Toriumi, K.; Ito, T.; Saito, A.; Nakagawa, I. *J. Phys. Chem. Soc. Jpn.* **1985**, *54*, 2184–2189.
(31) (a) Kohn, J. A.; Townes, W. D. *Acta Crystallogr.* **1961**, *A14*, 617–621. (b) Reynhardt, E. C.; Boeyens, J. C. A. *Acta Crystallogr.* **1972**, *B28*, 524–529. (c) Zhou, P.; Xue, F.; Au-Yeung, S. C. F. *Acta Crystallogr.* **1998**, *C54*, No. IUC9800062.
(32) (a) Nast, R.; Rehder, D. *Chem. Ber.* **1971**, *104*, 170–1713. (b) Bennett, B. G.; Nicholls, D. *J. Chem. Soc. A* **1971**, 1204–1206. (c) Müller, A.; Werle, P.; Diemann, E.; Aymonino, P. J. *Chem. Ber.* **1972**, *105*, 2419–2420. (d) Levenson, R. A.; Towns, R. L. R. *Inorg. Chem.* **1974**, *13*, 105–109. (e) Levenson, R. A.; Dominguez, R. J. G.; Willis, M. A.; Young, F. R., III *Inorg. Chem.* **1974**, *13*, 2761–2764.
(33) Blümel, J.; Hebendanz, N.; Hudeczeck, P.; Köhler, F. H.; Strauss, W. *J. Am. Chem. Soc.* **1992**, *114*, 4223–4230.
(34) Köhler, F. H.; Hofmann, P.; Prössdorf, W. *J. Am. Chem. Soc.* **1981**, *103*, 6359–6367.
(35) Baker, J. M.; Bleaney, B.; Bowers, K. D. *Proc. Phys. Soc., London, Sect. B* **1956**, *69*, 1205–1215.
(36) (a) Ljungström, E. *Acta Chem. Scand., Ser. A* **1977**, *31*, 104–108. (b) Eaton, J. P.; Nicholls, D. *Trans. Met. Chem.* **1981**, *6*, 203–206.
(37) Scholz, F.; Dostal, A. *Angew. Chem.* **1995**, *107*, 2876–2878.
(38) (a) Toyoda, H.; Niizeki, N.; Waku, S. *J. Phys. Soc. Jpn.* **1960**, *15*, 1831–1841. (b) Kiriyama, R.; Kiriyama, H.; Wada, T.; Niizeki, N.; Hirabayashi, H. *J. Phys. Soc. Jpn.* **1964**, *19*, 540–549. (c) Taylor, J. C.; Mueller, M. H.; Hitterman, R. L. *Acta Crystallogr.* **1970**, *A26*, 559–567. (d) Willans, M. J.; Wasylishen, R. E.; McDonald, R. *Inorg. Chem.* **2009**, *48*, 4342–4353.
(39) Recent examples are the following: (a) Telser, J.; Pardi, L. A.; Krzystek, J.; Brunel, L.-C. *Inorg. Chem.* **1998**, *37*, 5769–5769. (b) Garces, N. Y.; Giles, N. C.; Halliburton, L. E.; Nagashio, K.; Feigelson, R. S.; Schunemann, P. G. *J. Appl. Phys.* **2003**, *94*, 7567–7570.
(40) Figgis, B. N. *Trans. Faraday Soc.* **1961**, *57*, 204–209.
(41) O'Reilly, D. E.; Schacher, G. E. *J. Chem. Phys.* **1965**, *43*, 4222–4233.
(42) (a) Shulman, R. G. *J. Chem. Phys.* **1958**, *29*, 945–947. (b) Loewenstein, A.; Sporer, M.; Navon, G. *J. Am. Chem. Soc.* **1963**, *85*, 2855–2856. (c) Sporer, M.; Ron, G.; Loewenstein, A.; Navon, G. *Inorg. Chem.* **1965**, *4*, 358–361. (d) Davis, D. G.; Kurland, R. J. *J. Chem. Phys.* **1967**, *46*, 388–390. (e) McGarvey, B. R.; Pearlman, J. *J. Magn. Reson.* **1969**, *1*, 178–184. (f) Umehara, Y.; Hara, H.; Maruta, G. *Mol. Cryst. Liq. Cryst.* **2002**, *379*, 253–258. (g) Ishiyama, H.; Maruta, G.; Kobayashi, T.; Takeda, S. *Polyhedron* **2003**, *22*, 1981–1987. (h) Watanabe, R.; Ishiyama, H.; Maruta, G.; Kobayashi, T.; Takeda, S. *Polyhedron* **2005**, *24*, 2599–2606.
(43) Grey, C. P.; Dobson, C. M.; Cheetham, A. K. *J. Magn. Reson.* **1992**, *98*, 414–420.
(44) Harris, R. K.; Olivieri, A. C. *Prog. Nucl. Magn. Reson. Spectrosc.* **1992**, *24*, 435–456.
(45) (a) La Mar, G. N.; Horrocks, Jr., W. DeW.; Holm, R. H. *NMR of Paramagnetic Molecules*; Academic Press: New York, 1973. (b) Bertini, I.; Luchinat, C. In *Physical Methods for Chemists*; Drago, R. S., Ed.; Saunders College Publishing: Ft. Worth, TX, 1992; pp 500–556.
(46) (a) Weil, J. A.; Bolton, J. R.; Wertz, J. E. *Electron Paramagnetic Resonance*; Wiley Interscience: New York, 1994; Chapter 5. (b) Drago, R. S. In *Physical Methods for Chemists*; Drago, R. S., Ed.; Saunders College Publishing: Ft. Worth, TX, 1992; Chapters 9 and 13. Early original work: (c) Marshall, W.; Stuart, R. *Phys. Rev.* **1961**, *123*, 2048–2058 and references therein.
(47) Owen, J.; Thornley, J. H. M. *Rep. Progr. Phys.* **1966**, *29*, 675–728.
(48) (a) Nayeem, A.; Yesinowski, J. P. *J. Chem. Phys.* **1988**, *89*, 4600–4608. (b) Brough, A. R.; Grey, C. P.; Dobson, C. M. *J. Chem. Soc., Chem. Commun.* **1992**, 742–743. (c) Brough, A. R.; Grey, C. P.; Dobson, C. M. *J. Am. Chem. Soc.* **1993**, *115*, 7318–7327. (d) Lee, H.; Polenova, T.; Beer, R. H.; McDermott, A. E. *J. Am. Chem. Soc.* **1999**, *121*, 6884–6894. (e) Heise, H.; Köhler, F. H.; Xie, X. *J. Magn. Reson.* **2001**, *150*, 198–206. (f) Lee, Y. J.; Grey, C. P. *J. Phys. Chem. B* **2002**, *106*, 3576–3582.
(49) Herzfeld, J.; Berger, A. E. *J. Chem. Phys.* **1980**, *73*, 6021–6030.
(50) Harris, R. K.; Becker, E. D.; Cabral de Meneces, S. M.; Granger, P.; Hoffman, R. E.; Zilm, K. W. *Pure Appl. Chem.* **2008**, *80*, 59–84.
(51) Kurland, R. J.; McGarvey, B. R. *J. Magn. Reson.* **1970**, *2*, 286–301.
(52) Mohr, P. J.; Taylor, B. N. *Rev. Mod. Phys.* **2005**, *77*, 1–107.
(53) Vega, A. J.; Fiat, D. *Pure Appl. Chem.* **1972**, *32*, 307–315.
(54) Duelund, L.; Toftlund, H. *Spectrochim. Acta, Part A* **2000**, *56*, 331–340.
(55) (a) Brown, P. J.; Day, P.; Fischer, P.; Güdel, H. U.; Herren, F.; Ludi, P. *J. Phys. C* **1982**, *43*, 235–240. (b) Reynolds, P. A.; Delfs, C. D.; Figgis, B. N.; Moubaraki, B.; Murray, K. S. *Aust. J. Chem.* **1992**, *45*, 1301–1305.
(56) (a) Morton, J. R.; Preston, K. F. *J. Magn. Reson.* **1978**, *30*, 577–582. (b) Koh, A. K.; Miller, D. J. *At. Data Nucl. Data Tables* **1985**, *33*, 235–253.
(57) Watson, R. E.; Freeman, A. J. *Phys. Rev. Lett.* **1961**, *6*, 343–345.
(58) Ruiz, E.; Cirera, J.; Alvarez, S. *Coord. Chem. Rev.* **2005**, *249*, 2649–2660.
(59) Ruiz, E.; Rodrígues-Fortea, A.; Alvares, S.; Verdaguer, M. *Chem.—Eur. J.* **2005**, *11*, 2135–2144.
(60) (a) Atanasov, M.; Comba, P.; Daul, C. A.; Hauser, A. *J. Phys. Chem. A* **2007**, *111*, 9145–9163. (b) Atanasov, M.; Comba. *J. Mol. Struct.* **2007**, *838*, 157–163.
(61) Wolberg, A. *J. Chem. Phys.* **1971**, *54*, 1428–1430.